Langmuir

Article

pubs.acs.org/Langmuir

Self-Assembly of Mesoscopic Materials To Form Controlled and Continuous Patterns by Thermo-Optically Manipulated Laser Induced Microbubbles

Basudev Roy,[†] Manish Arya,[‡] Preethi Thomas,[§] Julius Konstantin Jürgschat,[§] K. Venkata Rao,[∥] Ayan Banerjee,*[,†] Chilla Malla Reddy,*[,‡] and Soumyajit Roy*[,§]

[†]Department of Physical Sciences, Indian Institute of Science Education Research, Kolkata (IISER-Kolkata), Mohanpur 741252, India

[‡]Department of Chemical Sciences, IISER-Kolkata, Mohanpur 741252, India

[§]EFAML, Materials Science Centre, Department of Chemical Sciences, IISER-Kolkata, Mohanpur 741252, India

[∥]JNCASR, Bangalore 560064, India

Supporting Information

ABSTRACT: The formation of continuous patterns of nanostructured materials using directed self-assembly under external fields has generated considerable current research interest. We demonstrate for the first time such continuous patterning by inducing irreversible self-assembly leading to nucleation in mesocopic materials (inorganic, organic, and nanoparticles) using a tightly focused laser beam in an optical tweezers apparatus. A dense aqueous dispersion or solution of the material which has high absorption at the laser wavelength is taken in a sample holder so that some material is adsorbed on the top surface. A hot spot is created on the top surface when the adsorbed material absorbs the high intensity at the focus of the laser beam (a submicrometer sized spot), due to which a water vapor bubble is formed. This causes self-assembly of material around the bubble due to Gibbs–Marangoni convection and capillary flow after which the material eventually nucleates into a crystalline state. The bubble is "trapped" at the hot spot due to the temperature gradient around it and can be manipulated by thermal forces generated optically, so that the system may be described as a "thermo-optical" tweezers. We translate the trapped bubble using the microscope sample holder stage of the apparatus so that the nucleation site of the material is simultaneously translated generating continuous patterns. We have demonstrated the technique using exotic inorganic materials such as soft oxometalates, an organic material such as glycine, and a fluorescent dye such as perylene as well as with carbon nanotubes. We have written patterns over lengths of nearly 1 mm at the rate of 1 Hz, with best resolution of about 4 μm. The technique has potential for a wide range of applications ranging from solution processed printable electronics to controlled catalysis.

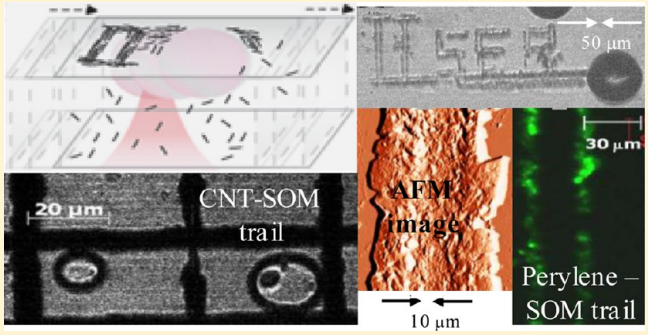

INTRODUCTION

Self-assembly strategies in nature have been studied and also adapted widely by scientists particularly in the mesoscale, where diverse applications have been found in nanotechnology,[1−5] molecular electronics,[6] etc. Self-assembly due to external stimuli is especially interesting,[7] since it allows control of the final structures by changing parameters of the stimuli. In this context, light is a very good choice as the external stimuli, since it can be tuned in many different ways—in terms of total intensity, wavelength, and spatial distribution of the intensity (Gaussian and/or higher order light beams). Thus, light assisted and controlled self-assembly has led to new structures as well as materials,[8−10] with multifarious applications in sensing,[11] delivery,[12] and optics.[13] For example, light introduced self-assembled suprastructures of nanoparticles have been shown to be disassembled for low concentrations of the nanoparticles by changing the light wavelength, while for high particle concentrations, permanent cross-linked structures are formed.[14] Recently, a lot of interest has been generated in the use of directed fields in order to form multiscale patterns using nanostructured materials,[15] while some success has been achieved in the formation of chains and networks of gold nanocrystals[16]—making continuous and long (millimeter scale) patterns using mesoscopic material has proved elusive.[15] In this context, some preliminary work has been performed in the growth of single crystals starting from a solution of nanomaterials by exploiting nucleation around an interface—which in several cases has been an air bubble grown in the solution.

Received: July 20, 2013
Revised: October 28, 2013
Published: October 30, 2013

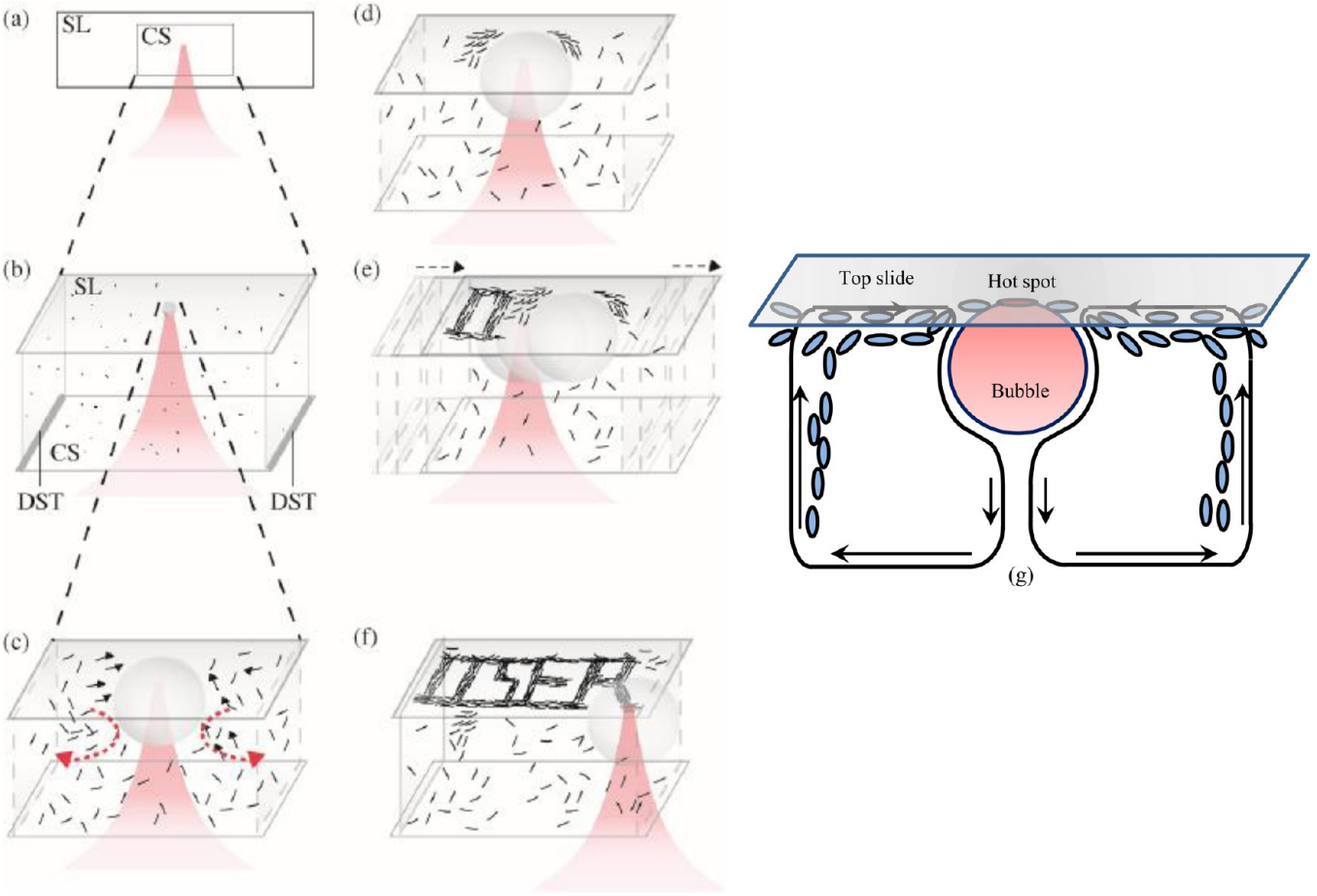

Figure 1. Schematic of the technique used for patterning. (a) Sample holder consisting of a top microscope slide (SL) and bottom coverslip (CS) attached to each other by a double-sided tape (DST shown in (b)). The sample holder contains an aqueous solution/dispersion of the material. The holder is placed on the automated precision scanning stage of an inverted microscope. A Gaussian beam (shown in red) is focused tightly near the top slide to form the optical tweezers. (b) The region around the coverslip zoomed in. The liquid has local density maxima of the dispersed soft material, where absorption from the focused laser beam is high—thus, a hot spot is created on the slide giving rise to a water vapor bubble. A single bubble formed by the coalescence of several microbubbles is shown. (c) The region around the bubble zoomed in. The temperature gradient in the vicinity of the bubble gives rise to strong Gibbs–Marangoni convection currents shown in red dashed arrows. The circulating currents cause self-assembly of soft material (SOM nanotubes and/or other species) toward the bubble which is shown by black arrowheads attached to the individual particles. (d) The soft material gradually assembles at the base of the bubble (in the form of a ring which is not shown) and undergoes a phase transition to enter into a crystalline phase. (e) The sample chamber is then translated controllably by scanning the microscope scanning stage. The deposition of material at the base of the bubble ensures that the laser "hot spot" moves concomitantly due to continuous absorption by the material, thus causing thermocapillary migration of the bubble, a process which continuously deposits fresh material at the bubble base. A continuous trail of crystalline (hard) material is therefore formed. (f) The microscope scanning stage can be moved horizontally and vertically to form a pattern of the word "IISER" with the nucleating material using a single bubble. (g) The cartoon explicitly demonstrates the direction in which Gibbs–Marangoni convection occurs around the bubble formed due to the hot spot. Particles are drawn in toward the bubble base due to Marangoni flow as well as the capillary flow created as a result of water evaporating near the bubble.

Thus, colloidal crystals have been reversibly formed by the directed assembly of colloidal nanoparticles in solution using bubble-mediated nucleation by an electric field.[17] More recently, single crystals of glycine[18] have been grown from solution—once again using bubble-mediated nucleation, but on this occasion the bubble was created due to the formation of a "hot spot" or high temperature region produced by a laser beam focused on a gold surface that was part of the sample holder for the solution. Discrete (noncontinuous) patterns of cadmium selenide quantum dots have also been achieved using a similar technique, where a bubble grown in the quantum dot dispersion around a "hot spot" produced by a focused laser on the gold substrate led to the self-assembly of the quantum dots on the substrate due to Gibbs–Marangoni convection,[19] while single-walled carbon nanotubes have been deposited on electrode edges using a similar technique.[20] This raises several important questions: Can continuous patterns be formed by directed self-assembly of nanostructured or, in general, mesoscopic materials? Can the patterning be completely controlled, fast (less than a second, note that the time scales in ref 18 was in the order of tens of seconds), and not depend on a particular choice of surface (such as gold as used in refs 17 and 18)? Also, while continuous mesoscale patterns have obvious applications such as the formation of optoelectronic circuits, is it possible to pattern exotic material such as transition metal oxides that have known catalytic activity,[21] so that one could perform highly specific and selective catalysis in the mesoscale? Recently, a class of metal oxide based mesoscopic structures (soft oxometalates)[22] have been discovered that can be formed from well-defined nanoscopic

dx.doi.org/10.1021/la402777e | *Langmuir* 2013, 29, 14733–14742

molecular polyoxometalate building blocks with unusual properties and applications in materials science and catalysis. These could therefore be well-suited as materials that could be used to synthesize controlled patterns in microscale where the structure is known until the last atomic detail. Thus, can the patterning be extended to soft oxometalates using them as building blocks?

In this paper, we have attempted to answer these questions by reporting a controlled and continuous optical patterning technique using self-assembly followed by nucleation around a bubble generated thermo-optically in an optical tweezers setup (see Figure 1, which is a cartoon depicting our technique). In an earlier work, we have shown reversible self-assembly of micrometer-sized polystyrene beads in the form of stable ring structures in an optical trap by the use of a predesigned optical field at the trapping plane.[23] Here, we present irreversible self-assembly of material of similar length scales, albeit by a different process altogether, in order to form continuous permanent patterns of the material on a glass substrate. We have formed patterns using three classes of materials: (1) a class of newly synthesized dispersed soft oxometalate (from here onward abbreviated as SOM)[22] nanotubes having high absorbptivity at λ = 1064 nm ($\sim 10^5$/mol cm^{-1}) resulting from a ligand metal charge transfer (LMCT) type transition, (2) organic molecules such as glycine and paracetamol, and (3) paracetamol, fluorescent dyes (such as perylene where the pattern can be illuminated under light), and carbon nanotubes (CNTs) loaded on the SOMs to demonstrate assisted nucleation. We observe that the patterning method is virtually independent of a particular choice of surface since we depend on the absorptive properties of the material in question in order to create a hot spot on the substrate around which the bubble grows. Subsequently, continuous patterns can indeed be formed using the SOMs and at much lower powers than that typically employed in laser-induced nucleation.[24−26] Patterns are also formed using organic molecules which have negligible absorbance at the laser wavelength, thus requiring much higher laser power. However, when the molecules are anchored on the SOMs, we observe assisted nucleation exploiting the excitation of SOM core due to LMCT type transition when exposed to the intense laser tweezers beam. The organic molecules have been chosen keeping in mind the presence of hydrogen bonding and coordination sites. This technique is much simpler, easily controllable, and fast (time scales less than 1 s presently achieved for writing 1 mm long line patterns) for any optical patterning scheme. We perform a detailed analysis of the factors affecting the technique using diverse material systems and different operating conditions so as to optimize the technique for wide applicability as a solution-based patterning process.

EXPERIMENTAL METHODS

Thermo-Optical Tweezers. The patterning is performed over a surface where a high density aqueous solution or dispersion of the material to be patterned is exposed to a thermo-optical tweezers that consists of a CW laser beam focused to a diffraction limited spot using a high numerical aperture objective lens.[27] The thermo-optical tweezers is constructed around an inverted microscope (Zeiss Axiovert. A1 Observer). A 100×, 1.4 N.A. oil immersion microscope objective (Zeiss plano-apochromat, infinity corrected) is used to couple 1064 nm light from a diode laser (Lasever LSR1064 ML) into the sample holder to attain a spot size of waist radius ∼500 nm. The laser power can be varied from 0 to 100 mW after the objective. The sample solution/dispersion is placed or sandwiched in a chamber consisting of a 1 mm thick standard glass slide (top surface) and a 160 μm thick glass coverslip (bottom surface) with double-sticking tape on the sides to control the spacing. Both surfaces are carefully cleaned with methanol and dried before each experimental run so as to eliminate the possibility of the presence of unwanted adsorbed material. About 75 μL of solution is inserted into the holder, which is then placed in the microscope scanning stage which is stepper motor controlled with a Ludl MAC5000 XY stage controller operated using a joystick. The total travel range is 130 × 100 mm with resolution of 100 nm. The process of crystallization is observed using a CCD camera (Axiovision) running at a fastest rate of 30 frames/s. Imaging is performed at the back focal port of the microscope using a combination of 10×/40×/100× objectives and external optics arranged outside the microscope.

Raman Spectrometer. Raman spectroscopy of the pattern inscribed on the top slide of the sample holder was performed in a commercial Raman microspectrometer (Horiba Jobin Yvon LABRAM HR800). The excitation laser was at 633 nm, and the top slide was placed on the Raman microscope stage for observing the Raman spectrum after it was carefully extracted from the sample chamber.

AFM. AFM studies of the patterns were performed in a NT-MDT, NTEGRA system with resolution ∼1 nm. The solution in the sample holder was allowed to dry off naturally, and the top slide was carefully removed so as to not damage the pattern inscribed on it.

Synthetic Procedure. *a. Molybdenum-Based Soft Oxometalate.* The SOM was prepared by dispersing 817.6 mg of ammonium heptamolybdate tetrahydrate (from Sigma-Aldrich) in 4 mL of water which was warmed until a homogeneous dispersion was obtained that scattered light from a laser. This dispersion was then cooled to room temperature before being used for optical patterning experiments.

b. Glycine. The high density solution of glycine (from Sigma-Aldrich) was made by dissolving 65 mg of glycine in 0.5 mL of water and sonicating it for 1 min.

c. Perylene. 5 mg of perylene (from Sigma-Aldrich) was dissolved in 0.5 mL of water and sonicated for 1 min.

d. SOM with Paracetamol. Ammonium heptamolybdate tetrahydrate (817.6 mg) was dissolved in 4 mL of water and was warmed until a homogeneous dispersion was obtained. This dispersion was then cooled to room temperature. Paracetamol (10 mg) was added to this dispersion in the mole ratio 1:10.

e. CNTs. Single-walled CNTs were prepared using standard techniques. The average diameter of the CNTs was 1.2 nm and length around 1 μm.

f. SOMs with CNTs. CNTs were physically mixed with SOMs and were subjected to the tweezer setup for patterning. A mole ratio of 1:10 for CNT:SOM works well for this patterning.

RESULTS AND DISCUSSION

Choice of Materials and Solvent. The technique, as mentioned earlier, depends on the growth of a bubble around a hot spot formed at the laser focus region on the sample chamber. Our choice of materials is driven by the necessity to form hot spots with minimum dependence on surface properties. Hence, absorption of the material could help in hot spot formation without the need for intricate surface modification. For this reason, SOMs were ideal for our present methodology. SOMs[22] are a class of materials that have a diffuse or soft interface and have colloidal length scales and are comprised of several thousands of oxometalate building blocks stitched by supramolecular interactions. Several such SOMs have been synthesized by us and others.[22] Some SOMs are spontaneously formed,[28−30] while other formations are directed, using colloidal structural directing agents.[31,32] In this work, we synthesize SOM nanotubes (molybdenum based) and form patterns using a dispersion of such tubes and also use them individually as templates for loading organic materials and carbon nanotubes (see later). They are characterized in detail

dx.doi.org/10.1021/la402777e | Langmuir 2013, 29, 14733−14742

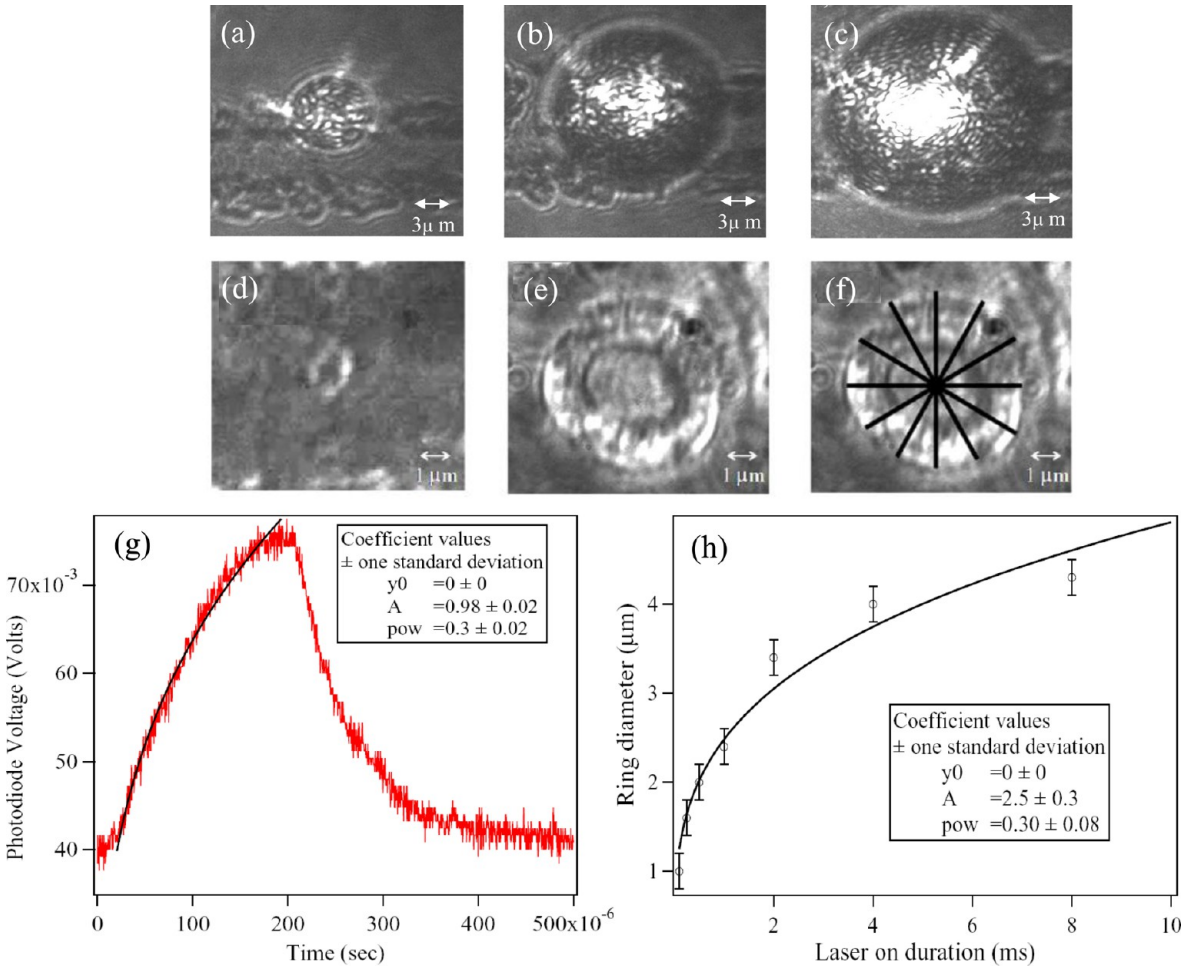

Figure 2. (a) Diameter of steady-state bubble as a function of laser power—in this case the power is around 35 mW, the corresponding diameter being around 6 μm. (b) Bubble for power of 60 mW; diameter is now around 15 μm. (c) Bubble for power of 110 mW; diameter is now around 20 μm. Note that the same effects would be obtained if the laser is kept on for different exposure times at the same power level. (d) A ring of deposited SOMs, now in the crystalline state. The trapping laser has been turned on for 100 μs. The ring diameter is around 1 μm. (e) Ring of deposited SOMs with the laser turned on for 8 ms; the diameter has now increased to around 4.5 μm. (f) Determination of the diameter of the ring formed by deposition of the nucleating material. Since the ring is not exactly annular, we measure the diameter at six locations covering the entire manifold and take an average. (g) Ostwald ripening in action: plot of bubble diameter vs time for a fixed laser power. A measurement laser is incident on the bubble as it grows (diameter of the spot is bigger than the bubble), and the scattering is detected on a photodetector. The rate of growth again follows a power law with an exponent of 0.30(2), which signifies that this is a manifestation of Ostwald ripening of the bubble at late times. The laser is switched off after 200 μs, and the decay process of the bubble is also recorded on the photodetector. (h) Plot of ring diameter vs laser on duration. The increase of the diameter follows a power law behavior with time, with a fit exponent of around 0.30(8). This is again clearly indicative of an Ostwald ripening process occurring in the nucleating material as the laser is kept on for longer periods of time.

by microscopic and spectroscopic techniques. To check whether this method works with organic molecules having poor absorptivity in the IR region, we used glycine and paracetamol solutions in water and observed that hot spots and thereby patterns could be formed in that case as well, albeit by using almost 5 times higher power for the trapping laser. It was also observed that certain materials such as CNTs did not form patterns due to poor adherence to the surface after they self-assembled on it. However, for these cases, as well as for organic molecules including a fluorescent dye, perylene, we loaded the material as a substrate on the SOMs and were able to form patterns quite easily (and at much lower laser powers for the organic molecules) using the high absorptivity of the SOMs. Note that all the organic molecules chosen have hydrogen bonding and coordination sites available to bind with the SOMs, while CNTs have a physical interaction with the SOMs under the tweezer setup. The role of SOMs in patterning is of assisted nucleation and with the goal of forming composite mesoscopic structures.

We choose water as a solvent mainly due to the fact that transition metal oxides with LMCT bands and several other organic molecules with coordinating groups dissolve readily in water. SOMs, on the other hand, disperse in water. In addition, given the need for a cheap and green solvent, water becomes a natural choice. Hence, the technique used here could be employed for cheap and eco-friendly electronic printing.

Nucleation Process. *Bubble Nucleation.* For best results, the trapping laser is focused on the top slide. Some of the SOMs in the aqueous dispersion are adsorbed on the top slide, and when the focused laser beam is incident on such adsorbed SOMs, hot spots are formed on the top slide due to the high absorptivity of the SOMs at 1064 nm. Such a hot spot is located by an initial scan of the microscope stage. Several water vapor microbubbles are formed in the vicinity of the hot spot in time

dx.doi.org/10.1021/la402777e | *Langmuir* 2013, 29, 14733−14742

scales of the order of microseconds. It is interesting to note that a similar hot spot is also formed when the laser is focused at the bottom surface (coverslip), but bubbles formed in that region would be pushed upward immediately by buoyant forces so that nucleation would not occur at all. However, the microbubbles formed near the top slide immediately coalesce to form a large bubble following classical nucleation process,[33] and the single bubble grows in size very quickly (again in tens−hundreds of microseconds depending on the laser intensity). Now, the difference in temperature at the top and bottom surface of the bubble leads to a difference in surface tension (which goes inversely as temperature), thus bringing about the well-known Gibbs−Marangoni convection flow of liquid around the bubble. Additionally, a capillary flow due to evaporation of water[34] also sets in as we have demonstrated in Figure 1g. Thus, particles in solution are drawn toward the bubble. The top slide acts as a boundary surface for the flow and the particles self-assemble at the "bubble base"—which is essentially the contact area of the bubble on the top slide−in the form of a ring.[19] Note that this assembly occurs only in the presence of a bubble. In its absence, even with the trapping laser focused on the top surface, we do not observe any assembly at all. We demonstrate the flow of particles due to convection currents induced by the bubble in Video 1 for polystyrene beads of diameter 3 μm—the beads are seen to flow in gradually toward the bubble initially and are suddenly pulled toward it due to the strong flows that exist around the bubble. The flow velocities of the beads near the bubble have been measured to be more than 50 μm/s by frame by frame analysis of the videos, and this is much higher than the flow velocities observed in the absence of the bubble but with the laser focused on the top slide. This proves that normal thermal convection cannot be responsible for the self-assembly of material around the base of the bubble.

There is also a direct evidence of bubble nucleation by Ostwald ripening which we monitor by measuring the rate of growth of a bubble by coupling a detection laser at 670 nm into the trapping microscope and measuring the light scattered from the bubble on a photodiode. The trapping laser power was blinked or on/off modulated by an acousto-optic modulator (AOM) for controlled time periods (a few hundred microseconds), while the detection laser was constantly on. The spot size of the detection laser was kept to around 5 μm, which was much bigger than the sizes typically reached by a bubble in the time scales during which the trapping laser remained on. The growth of a bubble with laser power is shown in Figure 2a−c where we show bubbles at laser powers of 35, 60, and 110 mW, with the bubble sizes being 6, 15, and 20 μm, respectively. Note that these are bubbles reaching steady state and do not reflect the sizes the bubble would reach during the time the laser beam is kept on for the modulation experiments. Figure 2g shows the scattered intensity with time when the trapping laser is kept on for 200 μs. The bubble growth clearly follows a power law in time, with the exponent being 0.30(2), which demonstrates the onset of Ostwald ripening at late times.[32] The plot also shows how the bubble diameter decreases as the bubble shrinks when the laser is turned off.

Crystal Nucleation. It is interesting to note that when the laser is turned off, the material ring (viscous) formed at the bubble base undergoes a soft-to-crystalline phase transition that ultimately forms crystals.[18] This is a second nucleation process—different from the bubble nucleation that we demonstrate with the measurement of light scattered off the bubble as it is growing. For studying the dynamics of this process, the trapping laser power was once more on/off modulated by the AOM for controlled time periods. We increased the laser on-time gradually and measured the size of the material ring deposited at the base of the bubble and plotted the increase in ring diameter with increasing laser on-times (Figure 2d,e). The ring diameter was measured by using reference polystyrene beads of known diameter stuck to the glass slide. The final diameter calculated was the average of six different estimates at different locations along the entire manifold of the ring. (Figure 2f) The plot of ring diameter as a function of time is shown in Figure 2h. Note that the material ring is essentially the footprint of the bubble and would therefore carry the signatures of Ostwald ripening. A fit to the data (ring diameter against time) yields a power law behavior with an exponent 0.30(8)—which strongly demonstrates Ostwald ripening (Figure 2h). This is consistent with the two-stage crystal nucleation theory where the end of the first stage is manifested by a phase transition from a viscous soft state to a crystalline hard state of matter.[35−37] The crystallization is also verified using Raman spectroscopy (Figure 3). Note that we use the SOMs to study this phase transition since they are most easily patterned. Clearly there are two steps in this process, viz., (i) accumulation of the SOMs in dispersion (described previously) by the trapping laser and (ii) their transition to crystalline oxometalates when the trapping laser is turned off. The Raman spectra of the SOMs in dispersion have an intense Mo−O_{br}−Mo band at around 938 cm^{-1}, which is due to the breathing mode of the SOM nanotubes in dispersion (Figure 3a).[28] However, on crystallization this band almost disappears, whereas an intense Mo═O_t band is observed as in crystalline state these modes are active and numerous, which implies that crystallites of oxometalates are formed in the optical field (Figure 3b).

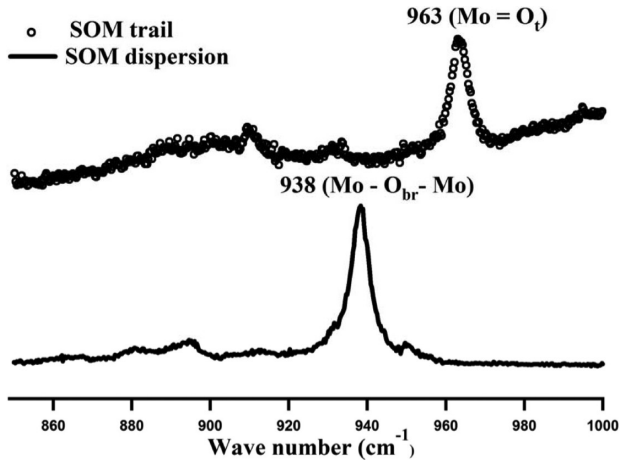

Figure 3. Raman spectral patterns: (a) Raman spectra of SOMs in an aqueous dispersion (solid line) and (b) Raman spectra of the trails in a bubble-induced trail (open circles). The Raman spectra of the SOMs in aqueous dispersion have an intense Mo−O_{br}−Mo band at around 938 cm^{-1}, which is due to the breathing mode of the SOM nanotubes in dispersion.[21] However, on crystallization, this band disappears whereas an intense Mo═O_t band is observed at 963 nm, thus implying that crystallites of oxomolybdates are formed due to the trapping beam. On other locations of the slide, spectra of adsorbed SOMs (with a peak around 938 cm^{-1}) are observed, but no traces of other material are found.

dx.doi.org/10.1021/la402777e | *Langmuir* 2013, 29, 14733−14742

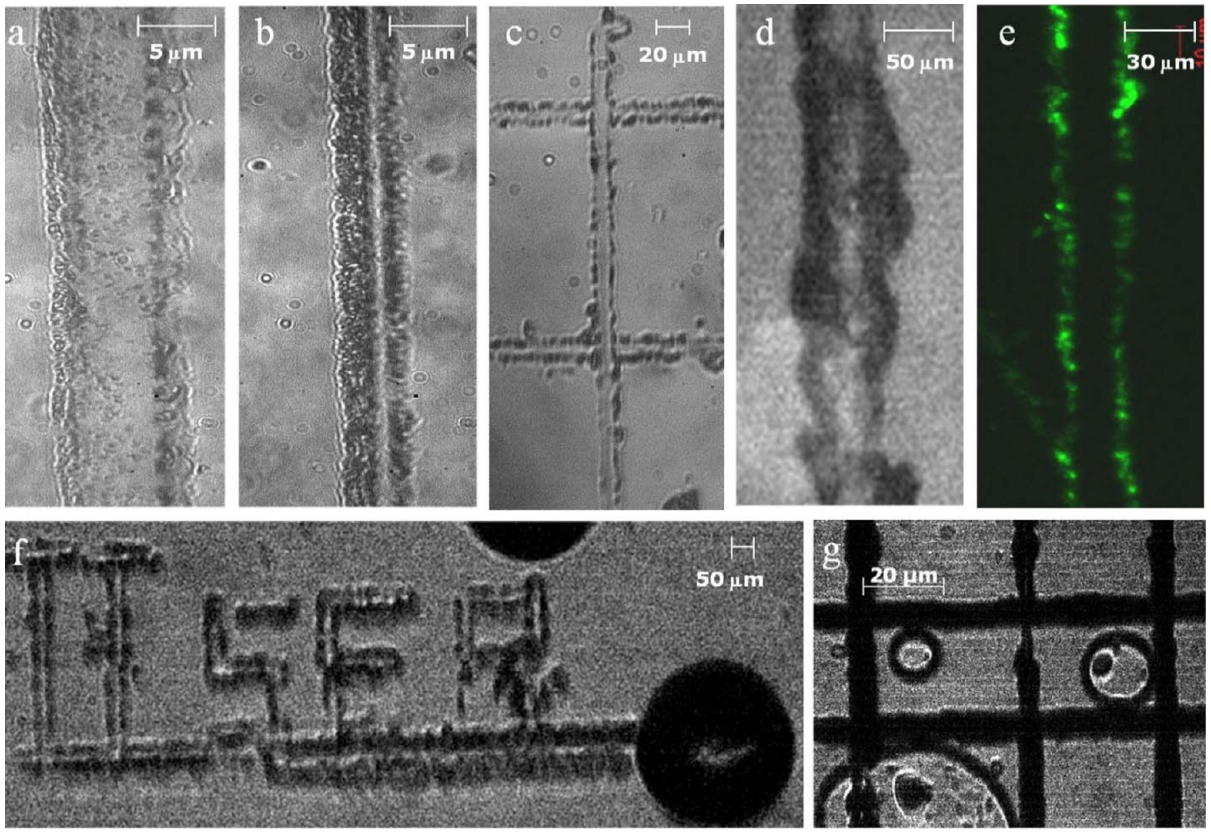

Figure 4. Pattern formation by nucleation: (a) Linear pattern of SOMs formed by controlled thermocapillary migration of a bubble in a dispersion of SOM nanotubes. A continuous trail is formed having width of around 8 μm at 50 mW laser power. (b) Same pattern at lower laser power of around 26 mW. The trail width has subsequently reduced proportionally to around 4 μm. (c) A double-cross pattern formed using SOMs. The trail thickness is around 15 μm. (d) Linear pattern formed with glycine. Laser powers required are higher by around a factor of 5 compared to the SOMs to form a bubble and then to induce thermocapillary migration by scanning the microscope stage. Material trail width is around 50 μm. (e) Linear pattern formed with the dye perylene loaded on the SOMs. Green fluorescence is observed from the material trail when irradiating with a laser at 488 nm. Trail width is around 30 μm. (f) Pattern "IISER" written on the top slide with deposited SOM crystals using a single bubble that is shown at the lower right corner of the picture (at the edge of the letter "R"). The microscope scanning stage is translated horizontally and vertically in order to form the letters with the bubble following the stage movement continuously. Material is continuously crystallized in the wake of the bubble to form the pattern. (g) Grid pattern formed using CNTs loaded on SOMs. The dark color of the trail establish the presence of the CNTs in the trails. The trail thickness is around 8 μm spread over an area of around 80 × 60 μm. The trail width is somewhat nonuniform in both (f) and (g), especially near the letter R in (f), and in the central region of the grid in (g) due to the manual manipulation of the microscope stage.

Pattern Formation. After the bubble grows to a certain size, the laser spot is moved to a new position of the sample by scanning the sample holder translation stage. Now, the hot spot is concomitantly moved, and the bubble follows the hot spot due to Gibbs−Marangoni convection—a phenomenon that can be described as thermo-optic bubble migration. Bubble confinement at the trapping laser focal spot and subsequent thermocapillary migration of the bubble using a precoated substrate with absorbing material has been reported earlier[38]—however, in our method the need for precoating is eliminated, since material is continuously deposited at the base of the bubble and slightly adjacent to it, so that there is always an absorbing media present on the surface of the slide to create a hot spot when the laser is shifted away slightly from the bubble. The bubble could thus be described to be indirectly trapped by the focused laser beam due to the temperature gradient around it[38] and follows the beam as it is scanned at high rates (around 1 mm/s or even higher). Thus, the process is very much similar to conventional optical tweezers trapping and manipulating high refractive index microparticles. (Note that bubbles, having lower refractive index compared to the surrounding medium, would be repelled away from the focus of the trapping beam in the absence of the hot spot.) In fact, the trapping forces produced due to optically induced thermocapillary effect are much stronger than that can be produced by optical forces alone—this is established by the fact that we can translate the bubble at speed of a few mm/s. Such high velocities cannot be attained by the use of optical forces alone which is borne out by the fact that particle translation velocities more than few μm/s[39] are difficult to achieve in those cases.

As the bubble is translated using the micrometer stage, continuous self-assembly and subsequent crystallization of material (in these cases SOMs and other organic molecules) in contiguous rings occur, which finally forms the desired pattern whose width corresponds to the diameter of the rings. In other words, this is indeed the translation of a trapped nucleation site which continuously leaves a trail of crystallized material behind. A chosen pattern is then formed by scanning the stage in a particular predetermined manner (Figure 4). A video of the deposition process by scanning the microscope stage and thereby the bubble is shown in Video 2. The factors affecting pattern formation are described later. Note also that the process is much more simpler when one attempts to extend a pre-existing pattern. A bubble is very easily formed when the

dx.doi.org/10.1021/la402777e | *Langmuir* 2013, 29, 14733−14742

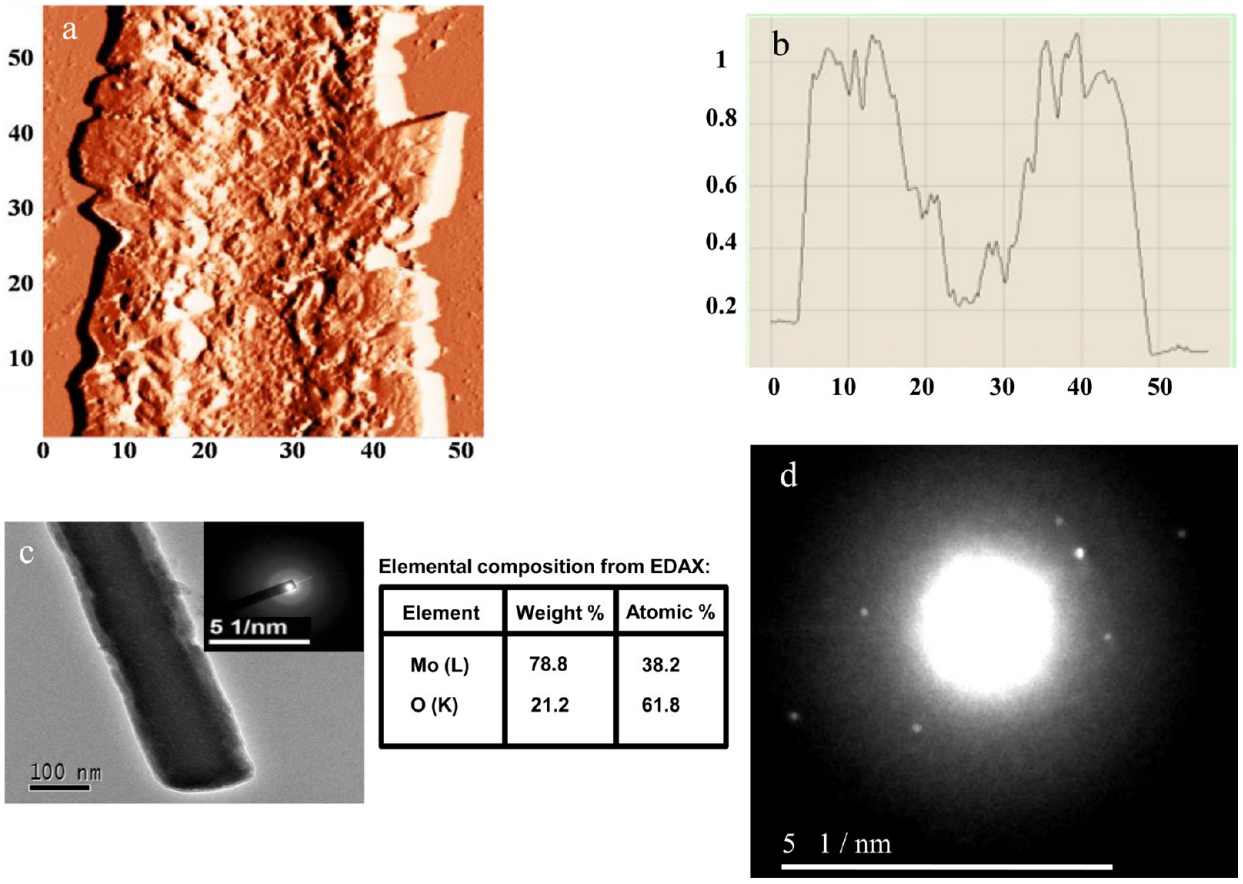

Figure 5. (a) AFM image of the trail. It shows continuous deposition of material with higher accumulation at the sides which is understandable since the material deposition would be lesser near the center where the bubble is in contact with the top slide. The trail width is around 40 μm with the dimensions of the *x*- and *y*-axes in micrometers. (b) *z*-scan for the same image gives a measure of trail depth which is around 1 μm. (c) TEM images of a single SOM nanotube, with EDAX showing the elemental constituents (provided in tabular form) of the pattern IISER that was written. SAED pattern (inset) shows noncrystalline nature of the nanotubes. (d) SAED pattern from the trail shows lattice reflections, thereby implying crystallinity which is not visible in (b).

trapping laser is focused to a pre-existing crystallized material trail because this acts as a seed to ensure faster formation of the nucleating site which can then be translated efficiently to cause further crystallization of material in a specified design.

For SOMs, the threshold for the bubble formation was found to be around 20 mW at the sample plane, which implied an intensity of only around 1.5 MW/cm^2 (more than an order of magnitude lesser than that reported in ref 24)—a factor that can be attributed to the high absorption levels observed in the electronic absorption spectra (EAS) of SOMs due to LMCT type transitions. Trails of crystallized oxometalate are shown in Figures 4a and 4b at different laser powers (40 and 22 mW, respectively). A more complicated double-cross structure has been shown in Figure 4c with the SOMs—the laser power used being around 70 mW. Continuous trails with deposited material were also obtained in organic molecules such as glycine (absorptivity at 1064 nm ~2500/mol cm^{-1}) and paracetamol (absorptivity at 1064 nm ~3000/mol cm^{-1}) using about 5 times higher laser power compared to the SOMs to compensate for the low absorption of the former at the laser wavelength. A trail formed with glycine is shown in Figure 4d. However, when paracetamol was loaded on the SOMs, the power threshold for nucleation reduced drastically to the same value as that with only the SOMs. In a similar exercise, carboxylate-substituted perylene (absorptivity at 1064 nm ~3000/mol cm^{-1}) was loaded on SOMs to form trails as is shown in Figure 4e, where the green fluorescence emitted from the dye when the pattern was irradiated with a laser of wavelength of 488 nm is also apparent. The fluorescence is higher at the edges of the trail than the center due to the fact that the self-assembly happens mostly around the bubble base in the form of rings as shown in Figure 2d,e. There is much lesser assembly at the center of the bubble since it is in contact with the slide near that region, and thus more dye is found at the edges than at the center of the trail. To demonstrate the power of the technique to produce complex patterns, we imprinted a pattern IISER on the slide with the SOMs by manually moving the microscope translation stage in the required manner (Figure 4f). The pattern thickness was around 50 μm while the total length of the pattern is around 1 mm. Finally, we produced patterns using CNTs that were again mixed in a dispersion with SOMs. Figure 4g shows a grid structure of width around 10 μm using the CNTs mixed with SOMs; the total area covered is around 80 × 60 μm, but this can be increased further as was demonstrated in case of Figure 4f. In addition, to verify the process of permanent deposition, AFM images were taken of the crystalline oxometalate patterns created in the top glass slide. As seen in Figure 5b, the AFM image confirms deposition of material to a thickness of about 1 μm on the slide. It is interesting to note that the thickness is higher on the two sides of the trail compared to the center, which confirms our assertion of self-assembly being much higher at the edges of the bubble. Figure

dx.doi.org/10.1021/la402777e | *Langmuir* 2013, 29, 14733−14742

5c shows TEM images of a single SOM nanotube, with EDAX (energy dispersive X-ray spectroscopy) showing the elemental constituents (provided in tabular form) of the material that was used to write the pattern IISER. The noncrystalline nature of the nanotubes is clear from the SAED (selected area electron diffraction) pattern that has been shown as an inset in Figure 5c. However, TEM performed on the trail indeed shows lattice reflections as is apparent in Figure 5d, which provides conclusive evidence to the fact that we indeed have material crystallization in all three dimensions using our process.

Factors Controlling Pattern Formation. We now describe in detail the factors that contribute to the formation of the pattern or more precisely the width of the pattern once the bubble is formed. These factors are as follows:

(i) *Laser Intensity and Time of Exposure of the Laser on the Sample*: The laser intensity along with the duration for which the laser is exposed to the sample directly controls the size of the bubble formed. The size of the bubble, in turn, determines the area over which material accumulation occurs and hence sets the width of the trail of deposited material. Such a difference in trail width for 22 and 40 mW laser power (focal spot size being the same) is shown in Figure 4a,b. For 40 mW power (Figure 4a), we observe a width of around 8 μm, which decreased to around 4 μm at 22 mW (Figure 4b)—in both cases the laser exposure time was about 0.5 s. This demonstrates that the amount of material deposition is proportional to laser intensity for the same exposure time. On the other hand, Figure 2d,e shows the increase in the size of the ring of the material deposited for the same laser power but for different exposure times, 100 μs and 8 ms, respectively. For exposure time of 100 μs, the diameter of the ring is around 1 μm, which is limited by the spot size of the trapping laser. Note that this is different from a continuous linear track, for which the best resolution obtained has been close to 4 μm as mentioned earlier, due to the fact that the microscope sample holder stage was translated manually so that the laser exposure time at a particular spatial location was longer than 100 μs.

(ii) *Speed of Moving the Translation Stage*: The speed of the stage essentially controls the time that the laser spends at a certain location, which determines the amount of material deposited on the substrate. Thus, to ensure uniform deposition of material and thereby uniform width of the trail, the stage is moved at close to constant velocity within manual operational limits. For instance, in the above experiments, the translation stage was moved manually at around 1 mm/s—the speed of translation being roughly calculated from the length of the trail divided by the total time taken to write it. The lack of uniformity in trail width is manifested in Figures 4f (near the letter R) and 4g (near the center of the grid pattern). Automation of the scanning process should remove such aberrations and ensure uniformity in this regard.

(iii) *Concentration of Materials*: The concentration of material in the solution controls the rate of self-assembly of material from the dispersion at the site of the bubble. Thus, for higher concentration samples, thicker trail widths would be obtained for similar laser power levels and exposure times. For example, the pattern IISER was written with a higher concentration sample compared to the rest of the trails shown in Figure 4, so that the trail width was higher in that case for exposure times similar to the other cases. In addition, for SOMs we observed bubble formation at around 0.1 M concentration (saturation concentration being around 0.3 M), whereas for the organic molecules, saturated solutions were used for trail formation. The reason was obviously the higher absorbance of SOMs compared to that of organic molecules.

Thus, the lowest resolution obtained in permanent patterns is around 4 μm—note that this could be improved further by manipulating the factors described above. In a nutshell, several methods such as using smaller bubbles (employing lower laser intensity), reducing the laser spot size by employing either a higher NA microscope objective or a smaller laser wavelength, or using low sample concentrations so that lesser material is assembled for a given laser power and exposure time could be employed to control the trail width. Presently, the best resolution that we obtain in the size of deposited material is around 1 μm, which is limited by the wavelength of the laser. It is also important to note that while we have shown self-assembly with SOMs exploiting their high absorptivity at 1064 nm, other materials should also be self-assembled provided the wavelength of the trapping laser is chosen to match the absorption wavelength of the material. In addition, patterning would also depend on whether the material would adhere to the substrate permanently as the SOMs.

Comparison with Other Patterning Techniques. There exist numerous other techniques for patterning at even nanoscales. These include X-ray lithography, photolithography including maskless lithography, double patterning, etc., electron-beam lithography, and scanning probe lithography—which provide spatial resolution from tens of nanometers even up to the atomic level. These techniques also allow stacking of different layers so as to provide complete three-dimensional control in patterning, which makes them useful in fabrication of logic gates and other electronic devices. However, these techniques are expensive, require elaborate preparation of the substrate (in terms of making masks) for creating the chosen pattern, and also typically take hours for completing the entire patterning process including the mask preparation and final developing. In contrast, our method is much faster, with millimeter long patterns being achieved in a few seconds. It requires no prior sample preparation with the only requirement being a laser that has a wavelength at which the material to be patterned has finite absorption. We have obtained thicknesses of around 1 μm, −and while the three-dimensional control is not as easy as for some of the above-mentioned techniques, it can be expected that high material concentration and larger dwell time of the laser at a certain spatial location would lead to thicker patterns. The issue of stacking multiple materials in a pattern remains to be investigated. Also, it is important to note that our technique is finally diffraction limited and the resolution of the patterns obtained would be ultimately dependent on the wavelength of the laser used, which implies that the best resolution that can be obtained would be around several hundred nanometers.

■ CONCLUSIONS

To summarize, we describe here an easily controllable and fast (patterning rates of around 1 mm/s in the present manual operation) method of light induced self-assembly of mesoscopic material that eventually leads to permanent patterns of the material over a surface. An important advantage of this patterning method is that it does not demand any special surface modifications. A high density aqueous dispersion/solution of the material to be patterned is taken in a sample holder and exposed to an optical tweezers system. The high laser intensity at the trapping laser focal spot accompanied by absorption of the material at the laser wavelength leads to the

formation of microbubbles that causes self-assembly of material from the liquid at the edges of the bubble due to Gibbs−Marangoni convection and evaporation induced capillary flow. The exposed region of the sample is then steered away from the laser spot using a scanning translation stage—the bubble follows the laser beam due to thermo-optic migration in a quasi-adiabatic manner so as to cause crystallization of the material in its wake on the overlying surface (top slide). Continuous patterns can be formed of the deposited crystals by steering the stage in a predetermined manner. The resolution for inscribing patterns can be controlled by the intensity of the laser in conjunction with the laser exposure time and material concentration in the dispersion/solution—presently, a resolution of around 1 μm has been achieved in depositing material over a glass substrate. We have patterned several materials including SOMs, organic molecules, and CNTs using this technique. SOMs have high absorbance at the wavelength of the trapping laser we use due to LMCT type transitions and can be patterned efficiently at much lower laser powers than has been used for patterning earlier.[26] In general, any organic substrate with hydrogen bonding site/s or coordination site/s or with complementary charges as that of SOMs can be used for patterning/writing. However, since these have quite low absorbance in the IR, the preformed SOM has been used as a template to load them in order to exploit the LMCT absorption to minimize the intensity required of the laser. The loaded molecules can also additionally bring in novel functionality. For instance, fluorescent probes and potential drug moieties can be incorporated as functionalities on the material. This method also shows that it is indeed possible to form patterns with well-defined precursors for microscopic SOMs, with the possibility of multifarious applications. The technique itself can have multiple and diverse applications ranging from printable electronics to controlled catalysis at the nano and micro scale. We are currently exploring some of these applications such as solution processed printable electronics[40,41] with water as well as other solvents in order to widen the scope of our technique. The technique can be improved on several counts but can be a first step toward efficient multiscale pattern formation of nanostructured materials by using directed self-assembly under controlled external conditions.

■ ASSOCIATED CONTENT

Supporting Information

Two videos providing a visual demonstration of different aspects of our technique: Video 1 shows the convective flow and subsequent assembly of polystyrene beads of diameter 3 μm at the base of the bubble. The bubble is grown at a pre-existing track by the laser tweezers beam. The bubble immediately causes an inflow of polystyrene beads toward it—the beads drift in gradually initially, but the velocity increases drastically as they near the bubble indicating the high flow velocities of water adjoining the bubble. The flow velocities measured near the bubble are more than 50 μm/s, which is much more than that can be achieved by simple thermal convection. This demonstrates Gibbs−Marangoni type of convection due to the bubble. Video 2 shows trail formation by a bubble. The bubble is translated at high speed (~1 mm/s) by scanning the microscope sample holder stage. Material self-assembly happens continuously in the wake of the bubble predominantly at the edges. This material is available free of charge via the Internet at http://pubs.acs.org.

■ AUTHOR INFORMATION

Corresponding Authors

*E-mail: ayan@iiserkol.ac.in (A.B.).
*E-mail: cmreddy@iiserkol.ac.in (C.M.R.).
*E-mail: s.roy@iiserkol.ac.in (S.R.).

Notes

The authors declare no competing financial interest.

■ ACKNOWLEDGMENTS

The authors gratefully acknowledge Dr. Subi George of JNCASR, Bangalore, for providing perylene, Dr. Harsh Chaturvedi of IISER Pune for providing CNTs, and Dr. Anindita Bhadra of IISER Kolkata for preparing Figure 1. They also acknowledge the financial support of Indian Institute of Science Education & Research, Kolkata. S.R. further thanks DST Fast track and BRNS for funding.

■ REFERENCES

(1) Gimi, B.; Leong, T.; Gu, Z.; Yang, M.; Artemov, D.; Bhujwalla, Z. M.; Gracias, D. H. Self-Assembled Three Dimensional Radio Frequency (RF) Shielded Containers for Cell Encapsulation. *Biomed. Microdevices* **2005**, *7*, 341−345.

(2) Leong, T.; Gu, Z.; Koh, T.; Gracias, D. H. Spatially Controlled Chemistry Using Remotely Guided Nanoliter Scale Containers. *J. Am. Chem. Soc.* **2006**, *128*, 11336−11337.

(3) Love, J. C.; Urbach, A. R.; Prentiss, M. G.; Whitesides, G. M. Three-Dimensional Self Assembly of Metallic Rods with Submicron Diameters Using Magnetic Interactions. *J. Am. Chem. Soc.* **2003**, *125*, 12696−12697.

(4) Gu, Z.; Chen, Y.; Gracias, D. H. Surface Tension Driven Self-Assembly of Bundles and Networks of 200 nm Diameter Rods using a Polymerizable Adhesive. *Langmuir* **2004**, *20*, 11308−11311.

(5) Erlebacher, J.; Aziz, M. J.; Karma, A.; Dimitrov, N.; Sieradzki, K. Evolution of Nonporosity in Dealloying. *Nature* **2001**, *410*, 450−453.

(6) Lindsey, J. S. Self-Assembly in Synthetic Routes to Molecular Devices. Biological Principles and Chemical Perspectives: A Review. *New J. Chem.* **1991**, *15*, 153−180.

(7) Roy, D.; Cambre, J. N.; Sumerlin, B. S. Future Perspectives and Recent Advances in Stimuli-Responsive Materials. *Prog. Polym. Sci.* **2010**, *35*, 278−301.

(8) Fialkowski, M.; Bishop, K. J. M.; Klajn, R.; Smoukov, S. K.; Campbell, C. J.; Grzybowski, B. A. Principles and Implementations of Dissipative (Dynamic) Self-Assembly. *J. Phys. Chem. B* **2006**, *110*, 2482−2496.

(9) Kim, A. J.; Biancaniello, P. L.; Crocker, J. C. Engineering DNA-Mediated Colloidal Crystallization. *Langmuir* **2006**, *22*, 1991−1995.

(10) Dassanayake, U.; Fraden, S.; van Blaaderen, A. Structure of Electrorheological Fluids. *J. Chem. Phys.* **2000**, *112*, 3851−3858.

(11) Oh, M.; Mirkin, C. A. Chemically Tailorable Colloidal Particles from Infinite Coordination Polymers. *Nature* **2005**, *438*, 651−654.

(12) Ecole, F.; Davisa, T. P.; Evans, R. A. Photo-Responsive Systems and Biomaterials: Photochromic Polymers, Light-Triggered Self Assembly, Surface Modification, Fluorescence Modulation and Beyond. *Polym. Chem.* **2010**, *1*, 37−54.

(13) Vossen, D. L. J.; Fific, D.; Penninkhof, J.; van Dillen, T.; Polman, A.; van Blaaderen, A. Combined Optical Tweezers/Ion Beam Technique to Tune Colloidal Masks for Nanolithography. *Nano Lett.* **2005**, *5*, 1175−1179.

(14) Klajn, R.; Bishop, K. J. M.; Grzybowski, P. A. Light-Controlled Self-Assembly of Reversible and Irreversible Nanoparticle Supra-structures. *Proc. Natl. Acad. Sci. U. S. A.* **2007**, *104*, 10305−10314.

(15) Grzelczak, M.; Vermant, J.; Furst, E. M.; Liz-Marzán, L. M. Directed Self-Assembly of Nanoparticles. *ACS Nano* **2010**, *4*, 3591−3605.

(16) Zhen, S. J.; et al. UV Light-Induced Self-Assembly of Gold Nanocrystals into Chains and Networks in a Solution of Silver Nitrate. *Nanotechnology* **2013**, *24*, 055601.

(17) Gong, T.; Wu, D. T.; Marr, D. W. M. Electric-Field Reversible Three-Dimensional Colloidal Crystals. *Langmuir* **2003**, *19*, 5967−5970.
(18) Uwada, T.; Fuji, S.; Sugiyama, T.; Usman, A.; Miura, A.; Masuhara, H.; Kanaizuka, K.; Haga, M. ACS Glycine Crystallization in Solution by CW Laser-Induced Microbubble on Gold Thin-film Surface. *ACS Appl. Mater. Interfaces* **2012**, *4*, 1158−1163.
(19) Fujii, S.; Kanaizuka, K.; Toyabe, S.; Kobayashi, K.; Muneyuki, E.; Haga, M.-A. Fabrication and Placement of a Ring Structure of Nanoparticles by a Laser-Induced Micronanobubble on a Gold Surface. *Langmuir* **2011**, *27*, 8605−8610.
(20) Takahashi, T.; Yabumoto, T.; Inori, R.; Okada, T.; Akita, S.; Arie, T. Electric Field Enhancement by Laser Light Focused at Electrode Edges for Controlled Positioning of Carbon Nanotubes. *Jpn. J. Appl. Phys.* **2012**, *51*, 06FD26.
(21) Wilkinson, G.; Cotton, F. A.; et al. *Advanced Inorganic Chemistry*; John Wiley & Sons Inc.: New York, 1998.
(22) Roy, S. Soft Oxometalates (SOMs): A Very Short Introduction. *Comm. Inorg. Chem.* **2011**, *32*, 113−126 and references therein.
(23) Haldar, A.; Pal, S. B.; Roy, B.; Gupta, S. D.; Banerjee, A. Self-Assembly of Microparticles in Stable Ring Structures in an Optical Trap. *Phys. Rev. A* **2012**, *85*, 033832.
(24) Sugiyama, T.; Yuyama, K.; Masuhara, H. Laser Trapping Chemistry: From Polymer Assembly to Amino Acid Crystallization. *Acc. Chem. Res.* **2012**, *45*, 1946−1954.
(25) Sun, B. A. G. X.; Myerson, A. S. Supersaturation and Polarization Dependence of Polymorph Control in Nonphotochemical Laser-Induced Nucleation (NPLIN) of Aqueous Glycine Solutions. *Cryst. Growth Des.* **2006**, *6*, 684−689.
(26) Zaccaro, J. M. J.; Myerson, A. S.; Garetz, B. A. Non-photochemical, Laser-Induced Nucleation of Supersaturated Aqueous Glycine Produces Unexpected γ-Polymorph. *Cryst. Growth Des.* **2001**, *1*, 5−8.
(27) Ashkin, A. Optical Trapping and Manipulation of Neutral Particles Using Lasers. *Proc. Natl. Acad. Sci. U. S. A.* **1997**, *94*, 4853−4860.
(28) Roy, S.; Planken, K. L.; Kim, R.; Mandele, D. v. d.; Kegel, W. K. Direct Evidence on the Existence of [Mo_{132}] Keplerate-Type Species in Aqueous Solution. *Inorg. Chem.* **2007**, *46*, 8469−8471.
(29) Roy, S.; Rijneveld-Ockers, M. T.; Groenewold, J.; Kuipers, B. W. M.; Meeldijk, H.; Kegel, W. K. Spontaneous Formation of Micrometer-Size Inorganic Peapods. *Langmuir* **2007**, *23*, 5292−5295.
(30) Roy, S.; Meeldijk, H. J. D.; Petukhov, A. V.; Versluijs, M.; Soulimani, F. Synthesis and Characterization of {$Mo_{72}Fe_{30}$}-coated Large Hexagonal Gibbsite γ-Al(OH_3) Platelets. *Dalton Trans.* **2008**, *21*, 2861−2865.
(31) Roy, S.; Mourad, M. C. D.; Rijneveld-Ockers, M. T. Synthesis and Characterization of Large Surface Hexagonal Polyoxometalate Platelets. *Langmuir* **2007**, *23*, 399−401.
(32) Roy, S.; Bossers, L. C. A. M.; Meeldijk, H. J. D.; Kuipers, B. W. M.; Kegel, W. K. Directed Synthesis of Stable Large Polyoxomolybdate Spheres. *Langmuir* **2008**, *24*, 666−669.
(33) Sagui, C.; Grant, M. Theory of Nucleation and Growth during Phase Separation. *Phys. Rev. E* **1999**, *59*, 4175−4187.
(34) Deegan, R. D.; Bakajin, O.; Dupont, T. F.; Huber, G.; Nagel, S. R.; Witten, T. A. Capillary Flow As the Cause of Ring Stains from Dried Liquid Drops. *Nature* **1987**, *389*, 827−829.
(35) Erdemir, D.; Lee, Y.; Myerson, S. Nucleation of Crystals from Solution: Classical and Two-Step Models. *Acc. Chem. Res.* **2009**, *42*, 621−629.
(36) Davey, R. J.; Schroeder, S. L. M.; ter Horst, J. H. Nucleation of Inorganic Crystals - A Molecular Perspective. *Angew. Chem., Int. Ed.* **2013**, *52*, 2166−2179.
(37) Vekilov, P. G. Nucleation. *Cryst. Growth Des.* **2010**, *10*, 5007−5019.
(38) Berry, D. W.; Heckenberg, N. R.; Rubinsztein-dunlop, H. Effects Associated with Bubble Formation in Optical Trapping. *J. Mod. Opt.* **2000**, *47*, 1575−1585.
(39) Ogura, Y.; Shirai, N.; Tanida, J. Optical Levitation and Translation of a Microscopic Particle by Use of Multiple Beams Generated by Vertical-Cavity Surface-Emitting Laser Array Sources. *Appl. Opt.* **2002**, *41*, 5645−5654.
(40) Dasgupta, S.; Stoesser, G.; Schweikert, N.; Hahn, R.; Dehm, S.; Kruk, R.; Hahn, H. Printed and Electrochemically Gated, High Mobility, Inorganic Oxide Nanoparticle FETs and Their Suitability for High Frequency Applications. *Adv. Funct. Mater.* **2012**, *22*, 4909−4919.
(41) Herlogsson, L.; Noh, Y.-Y.; Zhao, N.; Crispin, X.; Sirringhaus, H.; Berggren, M. Downscaling of Organic Field Effect Transistors with a Polyelectrolyte Gate Insulator. *Adv. Mater.* **2008**, *20*, 4708−4713.